Dynamic melt flow of nanocomposites based on poly-ε-caprolactam

Utracki, Leszek A.; Lyngaae-Jorgensen, Jorgen

Publisher's version / Version de l'éditeur:
https://doi.org/10.1007/s003970100211
Rheologica Acta, 41, 5, pp. 383-482, 2002-08-01

Rheol Acta (2002) 41: 394–407

ORIGINAL CONTRIBUTION

Leszek A. Utracki
Jørgen Lyngaae-Jørgensen

Dynamic melt flow of nanocomposites based on poly-ε-caprolactam

Received: 24 May 2001
Accepted: 27 August 2001

L. A. Utracki (✉)
National Research Council Canada,
IMI, Boucherville, QC,
Canada J4B 6Y4
e-mail: Leszek.utracki@nrc.ca

J. Lyngaae-Jørgensen
Dept. Chem. Eng.,
Technical University of Denmark,
Lyngby, Denmark

Abstract The dynamic flow behavior of polyamide-6 (PA-6) and a nanocomposite (PNC) based on it was studied. The latter resin contained 2 wt% of organoclay. The two materials were blended in proportions of 0, 25, 50, 75, and 100 wt% PNC. The dynamic shear rheological properties of well-dried specimens were measured under N_2 at T = 240 °C, frequency $\omega = 0.1$–100 rad/s, and strains $\gamma = 10$ and 40%. At constant T, γ, and ω the time sweeps resulted in significant increases of the shear moduli. The γ and ω scans showed a complex rheological behavior of all clay-containing specimens. At $\gamma = 10\%$ the linear viscoelasticity was observed for all compositions only at $\omega > 1$ rad/s, while at $\gamma = 40\%$ only for 0 and 25 wt% of PNC. However, the effect was moderate, namely decreasing G′ and G″ (at $\omega = 6.28$ rad/s; $\gamma = 50\%$) by 15 and 7.5%, respectively. For compositions containing >25 wt% PNC two types of non-linearity were detected. At $\omega \le \omega_c = 1.4 \pm 0.2$ rad/s yield stress provided evidence of a 3-D structure. At $\omega > \omega_c$, G′ and G″ were sensitive to shear history – the effect was reversible. From the frequency scans at $\omega > \omega_c$ the zero-shear relative viscosity vs concentration plot was constructed. The initial slope gave the intrinsic viscosity from which the aspect ratio of organoclay particles, $p = 287 \pm 9$ was calculated, in agreement with the value calculated from the reduced permeability data, p = 286.

Keywords Polymeric nanocomposites · Dynamic melt flow · Organoclay · Montmorillonite · Poly-ε-caprolactam · Platelets suspensions · Aspect ratio

Introduction

Polymeric nanocomposites (NC) are materials that contain dispersed nanometer-size particles in a single or multi-component polymeric matrix. The nano-particles can be lamellar, fibrillar, tubular, shell-like, spherical, etc. To ascertain good dispersion in a hydrophobic melt, they are usually reacted with organic compounds, e.g., sodium montmorillonite (Na-MMT) with an onium salt, forming organoclay.

The majority of commercial NC contain 2–10 wt% of organoclay. NCs have been prepared with virtually all commodity and engineering, thermoplastic and thermoset resins (Utracki and Kamal 2002). However, from the long list, the historically first and commercially the most important are NCs based on polyamides, especially on poly-ε-caprolactam (PA-6). It has been reported (Ube Industries 2000) that addition of as little as 2 wt% of organoclay (in relation to PA) increases the density by less than 1%, tensile and flexural modulus by 70 and 130%, respectively, HDT by 70 °C, and reduces oxygen and moisture permeability by 50%, flammability by 70%, etc. The NCs are being used in the transport, packaging, and aerospace industries (Dagani 1999).

From the fundamental point of view, the reinforcing effect of nano-particles is related to the aspect ratio, p

(ratio of fiber length or platelet thickness to its diameter), and to the particle-matrix interactions. Independent of the actual dimension, for $p \geq 5p_c$ the reinforcing effect is the same as of an infinitely large particle, increasing the strength of the composite to that of the platelet strength. The critical value of the aspect ratio, p_c, is given by the ratio of the tensile strength to the interfacial shear strength – for most polymeric composites $p_c \cong 100$ (Piggott 1980). The available organoclays have $p \cong 10$–2000. Evidently, the importance of p depends very much on the source (mineral or synthetic), method of preparation, and that of processing. High p-values are crucial for the NC that is to be used to reduce permeability, as well as for generation of anisotropic mechanical performance, but less so for, e.g., reduction of flammability (Gilman et al. 2000).

Preparation of organoclays for the use in polymers is a laborious and exacting process that starts with the purification of the ore, grinding, ion exchange, then intercalation and drying (Knudson and Jones 1992; Clarey et al. 2000). Thus the organoclay price is relatively high, namely for mineral and synthetic, respectively, 1.6 and 2.3 US$/kg to be compared with 2.9 US$/kg for PA-6 (all mid-2001 prices).

The technology of NC that is an object of this paper (abbreviated as PNC) has been described in several patents and articles from the Toyota Research Corporation (now Toyota Central R & D Labs.) and Ube Industries (namely Okada et al. 1988; Deguchi et al. 1992; Okada and Usuki 1995). To produce PNC, first Na-MMT was intercalated with 12-aminolauric acid in an aqueous medium, which increased the interlayer spacing from $d_{001} = 0.96$ nm (dry Na-MMT) to 1.3 nm. Next, the organoclay was dispersed in the monomer and polymerized – during the polymerization d_{001} increased to about 7 nm. The final exfoliation of clay platelets takes place during processing.

Because of its small thickness and large p, the exfoliated clay has the specific surface area of about 750–800 m^2/g. This high value is responsible for the large effects clay has on the NC performance. It has been postulated that the optimal nanocomposite structure consist of disordered, exfoliated clay platelets dispersed in a polymeric matrix. However, as the aspect ratio increases, the encompassed volume of the platelet increases with the cube of its diameter. Thus, platelets with high aspect ratio are characterized by a low value of the maximum packing volume fraction, $\phi_{m,plate} = (3/2p)\phi_{m,sphere} \cong 1/p$, above which they are unable to rotate freely, and locally have to orient parallel to each other (Utracki 1995). In consequence, as Okada and Usuki (1995) showed, the interlayer spacing hyperbolically decreases with increasing clay content (from 22 nm at 5 wt% to 5 nm at 25 wt% of clay).

The flow of PNC is sensitive to the dispersed particle size, shape, and surface characteristics as well as to the transient geometrical structure and complex interactions that involve the matrix polymer, clay, and a compatibilizer. Thus, rheology complements the traditional methods of NC characterization, such as X-ray diffraction (XRD), transmission electron microscopy (TEM), permeability, or mechanical testing.

Few rheological studies on NCs have been published. Krishnamoorti et al. (1996) reported on the dynamic and steady-state flow of polydimethylsiloxane (PDMS) containing up to 15 wt% layered silicate. Linear increase of the zero-shear viscosity (η_o) with silicate loading was observed, but at high rates of deformation the matrix viscosity was nearly recovered. Surprisingly, exfoliation reduced the enhancement of η_o. The authors also tested PA-6 with organoclay (PNC). This preliminary work was expanded in the following publication that considered behavior of PNC containing 2 and 5 wt% of organoclay and NC of poly-ε-caprolactone with up to 10 wt% of organoclay (Krishnamoorti and Giannelis 1997). Since these systems were obtained by intercalation followed by polymerization that engendered a direct bonding between MMT surface and macromolecules, the authors labeled them as "end-tethered polymer layered silicate nanocomposites". The G' and G'' moduli were found to increase with clay loading. Their power-law dependence in the terminal zone was different from that observed for homopolymers. At low frequencies the rheological response of samples containing high level of clay showed almost a solid-like response.

It is to be expected that the rheological behavior of the end-tethered systems will somehow differ from that in others where such direct bonding is missing. Thus, Hoffmann et al. (2000a) showed that tethering has a dramatic effect on the degree of dispersion and rheology. Two types of polystyrene-based nanocomposites were prepared. In the first the clay was intercalated with phenyl ethyl amine, while in the second with amine-terminated PS. In the first system clay was intercalated, in the second it was exfoliated. A plot of G' vs reduced frequency (ωa_T) showed that neat PS and PS containing intercalated clay nearly superposed one on top of the other, whereas the exfoliated nanocomposite showed a large increase of G' (especially at low ω), indicating a network formation.

In the following publication (Hoffmann et al. 2000b) melt flow behavior of NC based on polyamide-12 was studied. Two types of clay were used: synthetic fluoromica and mineral MMT. The clay was intercalated using either protonated amino dodecanoic acid (ADA) or water, then dispersed in ADA, which in turn was polymerized. The use of ADA-intercalated clay resulted in formation of end-tethered structure, with exfoliated silicate layers chemically bonded to the matrix. By contrast, the use of water as a swelling agent resulted in nanocomposites comprising exfoliated silicate layers well dispersed in the polymer matrix, but without

attached polymer chains. A stress-controlled rheometer was used in the dynamic mode with parallel plate geometry at frequency $\omega = 1$–25 rad/s. The data were collected within the linear viscoelastic region. The rheological behavior of the NCs differed from that of neat PA-12 matrix. The presence of a super-structure was deduced from the low frequency behavior. For PNCs with polymer molecules not bonded to the clay surface the flow mainly depended on the matrix with only a minor influence of clay (at least up to 4 wt% loading). Tethering enhanced G' and G'' by one and by one-half decade, respectively.

Schmidt et al. (2000) studied shear orientation of polymer-clay solutions during Couette flow, probed by birefringence and SANS. Thus, 3 wt% of synthetic hectorite (platelets: $d = 30$ nm and $h \cong 1$ nm) was dispersed in aqueous solution of 2 wt% polyethylene glycol (PEG, $M_w = 10^3$ kg/mol) at $pH = 10$ and an NaCl concentration of 10^{-3} mol/l. To account for the SANS and birefringence results, the authors postulated that the polymer chains are adsorbed onto the clay particles. The birefringence indicated a mechanical coupling between clay platelets and polymer; at low rates of shear, $\dot{\gamma} < \dot{\gamma}_{critical} \simeq 30(s^{-1})$ its value was dominated by clay platelets, but at high by polymer chains stretched in the flow direction. SANS data indicated that at $\dot{\gamma} > \dot{\gamma}_{critical}$ the flow is strong enough to induce orientation. The clay platelets (within aggregates, having diameter $d = 32$–233 nm) were oriented in the flow direction with the surface normal in the neutral (not radial) direction.

Linear viscoelastic flow of NCs based on polystyrene-polyisoprene diblock copolymer was studied by Ren et al. (2000). MMT was intercalated with dimethyl-dioctadecyl-ammonium. At >6.7 wt% of organoclay the low frequency data showed a pseudo-solid-like behavior, similar to that observed for exfoliated end-tethered nanocomposites. The behavior was attributed to the presence of anisotropic stacks of clay platelets, each stack randomly oriented vis-à-vis another, and forming a percolated 3-D network that was incapable of fully relaxing. The large-amplitude oscillatory shear was able to orient these structures and increase their liquid-like character.

Solomon et al. (2001) reported on the linear and nonlinear rheology of polypropylene (PP) based NCs with intercalated MMT (interlayer spacing 2.9 nm) The Na-MMT was first intercalated with several ammonium salts (interlayer spacing increased from 1.1 to 2.1 nm). The NCs were prepared in an internal mixer by melt compounding with 1.3–6.2% intercalated-MMT and maleic anhydride grafted-PP (MA-PP) (3 parts per 1 part of organoclay). Addition of clay significant increased G' and G''. To study the viscoelastic non-linearity the steady-state shear flow reversal was conducted. First, a PNC specimen was sheared for 300 s at the rate of shear $\dot{\gamma} = 0.1\,s^{-1}$ recording the value of the shear stress (σ_{12}), then the flow was stopped for a time, t_{rest}, and the specimen was re-sheared at the same rate of shear, but in the opposite direction. Characteristically the magnitude of the stress overshoot (σ_{max}) increased with t_{rest}. The master curve was constructed plotting $(\sigma_{max}/\sigma_\infty - 1)/c$ vs t_{rest} (where σ_∞ is the value of σ_{12} at long time and c is MMT loading). The authors concluded that an anisometric structure is responsible for the non-linear flow behavior.

Galgali et al. (2001) investigated creep behavior of melt intercalated NC of PP with organoclay and MA-PP. The latter was added at a ratio of either 0:1 or 1:1 in respect to organoclay. The NCs were characterized by TEM and wide-angle X-ray diffraction (WAXD) at $T = 200$ °C. The creep compliance at shear stresses, $\sigma_{12} = 10$ and 50 Pa was significantly lower for NCs containing MA-PP, and the effect increased with annealing. TEM and WAXD showed the presence of clay aggregates dispersed within the polymer matrix and a small amount of exfoliated platelets. The zero shear viscosity (η_o) strongly depended on clay content. The η_o of compatibilized NCs containing ≥3 wt% clay was at least three orders of magnitude higher than that of matrix resin and the uncompatibilized NC. Importantly, the large increase of η_o was not accompanied by any increase in the flow activation energy compared to the matrix polymer. The compatibilized NC also showed an apparent yield stress. This solid-like response of molten NC apparently originates not from macromolecules entrapped between clay platelets, but rather from the frictional interactions of clay aggregates. The addition of MA-PP did not significantly affect WAXD spectra, but had a significant influence on rheology. Its presence increased the probability of 3-D formation (the solid-like rheological response) to the level similar to that observed for the end-tethered chains. The responsible mechanism was not identified – it may be that the MA-PP enhanced exfoliation of clay platelets, but it could also form a third phase inside NC that formed a percolating 3-D network. Even in face of the WAXD results, the authors clearly prefer the first possibility – they postulated that clay platelets exfoliated upon addition of MA-PP to form bridges between the aggregates forming a 3-D percolating network. The creep was found sensitive to the microstructural changes occurring in the nanocomposite.

Recently Okamoto et al. (2001) studied the extensional flow behavior of polypropylene (PP)/clay NC containing 0.2 wt % MA-PP and 4 wt% MMT intercalated with stearyl ammonium ion via melt extrusion at 200 °C. TEM showed fine dispersion of the silicate stacks ca 150 nm long and about 5 nm thick, while according to XRD the interlayer spacing was only $d_{001} \cong 2.79$ nm. For the study the rotating clamps, Meissner-type elongational RME rheometer was used at 150 °C at Hencky strain rates $\dot{\varepsilon} = 0.001 - 1.0\,s^{-1}$. The linear viscoelastic

envelope of the stress growth function in elongation was about tenfold higher than that computed from shear flow. Furthermore, a strong strain hardening (SH) was observed. The former type of behavior is expected from the multiphase systems with yield stress; however the second is contrary to expectation – strain softening has been reported for composites (Takahashi 1996). Furthermore, unlike single-phase polymer melts, the low deformation rate ($\dot{\gamma} = \dot{\varepsilon} = 0.001\,s^{-1}$) stress growth functions of NC (in shear and elongation) increase with test time, $t \leq 300$ s, not showing a tendency of reaching a steady state. The authors concluded that flow-induced internal structure is different in shear than in elongational. TEM observations indicated that in specimen elongated at $\dot{\varepsilon} = 1.0\,s^{-1}$ the MMT platelets aligned perpendicularly to the stretching direction, but at $\dot{\varepsilon} = 0.001\,s^{-1}$ the platelet orientation was more random, with many plates aligned in the flow direction. In the later case, according to the authors a *house of cards*-like structure was created by flocculation, similar to that observed in low intensity shear flow.

In summary, the rheological studies in shear and elongation demonstrated that even at low clay loading NC flow is complicated: (1) at low deformation rates by a solid-like yield stress behavior, caused by a 3-D structure; (2) at high strains the clay platelets get oriented, which causes the shear viscosity to decrease nearly to that of the matrix. The later effect is particularly evident in the steady-state flow. Both effects are stronger for the end-tethered than for free platelets systems, especially at higher clay loading.

In the studies on polyamide-based NCs the unstable nature of the polycondensation-type polymeric matrix must be of concern. The tests must clearly separate effects caused by the changes in the matrix from these brought about by the presence of nano-filler. The present article summarizes results of the first stage of the PNC rheological studies. Thus, the first goal is to study the stability of the PA, PNC, and their mixture. The second goal is through systematic and quantitative studies of selected rheological functions to elucidate mutual influence of the microstructure and flow. Furthermore, the limiting conditions for onset of complex behavior are of interest.

Experimental

Materials

Polyamide-6 (PA) and nanocomposite (PNC) that was based on it were obtained from Ube Intl. (commercial grades PA1015B and PA1015C2, respectively). Characteristics of these resins are published (Ube Industries 2000). The PA has the same molecular weight as the PNC matrix resin. The latter was produced by the reactor exfoliation method with 2 wt% of organo-clay (equivalent to 1.6 wt% or 0.64 vol.% of MMT) (Okada et al. 1988; Deguchi et al. 1992; Okada and Usuki 1995).

The rheological properties of the following seven samples were measured (see Table 1): PA and PNC as received and five their mixtures compounded in a Werner-Pfleiderer twin-screw extruder (TSE) and re-pelletized: 1. PA, 2. PA with 25 wt% of PNC, 3. PA with 50 wt% of PNC, 4. PA with 75 wt% of PNC, and 5. PNC. Note that the two commercial resins were tested using "as received" and re-extruded PA and PNC specimens.

Drying

Before the rheological tests the PA and PA-based materials have to be dried to a standard level. Thus, pelletized samples were dried under vacuum at 80 °C for up to a week. The complex shear modulus at two frequencies vs drying time is shown in Fig. 1. Calculations show that after 48 h drying the rheological signal is 0.4% below the ultimate level for $t \to \infty$. Since a similar conclusion was reached using the weight loss method (Bureau 2001), these rheological data do represent removal of volatiles, not a chemical modification of PA-6.

Rheological tests

After drying (48 h at 80 °C under vacuum) the pellets were directly loaded into a controlled strain rate rheometer (ARES from Rheometric Scientific). Parallel plates of 25 mm diameter were used for the dynamic tests at T = 240 °C. For the specimens temperature stabilization, 3 min soak time was allowed. The time, strain, and frequency sweeps were carried out under a blanket of dry nitrogen. The data were reproducible within ±2%. To confirm some results, tests were also carried out using the Rheometrics Mechanical Spectrometer, RMS.

Results

Time sweeps

Time sweeps were carried out for 1 h at frequency $\omega = 6.28$ rad/s and strains $\gamma = 10$ and 40%. All seven

Table 1 Polynomial fit parameters for the time sweeps. The first five samples were re-extruded or compounded, the last two "as received"

PNC wt%	G'_1	G'_2	G'_3	$r_{G'}$	G''_1	G''_2	G''_3	$r_{G''}$
0 (PA-6)	39.388	0.040822	0.0000	0.99996	1926.9	0.55258	–4.5154e-05	0.99983
25	82.285	0.061125	0.0000	0.99993	2194.0	0.48794	–3.1387e-05	0.99977
50	152.88	0.079951	–2.6699e-06	0.99987	2560.4	0.50421	–3.4721e-05	0.99970
75	242.65	0.093212	–3.8080e-06	0.99978	2898.0	0.44210	–2.7627e-05	0.99939
100 (PNC)	321.27	0.095999	–4.2305e-06	0.99971	3133.3	0.37305	–2.2062e-05	0.99859
0 (PA-6)	35.839	0.047436	0.0000	0.99995	1918.2	0.65015	–4.9298e-05	0.99958
100 (PNC)	559.74	0.17737	–1.0141e-05	0.99962	3773.2	0.54600	–2.8488e-05	0.99888

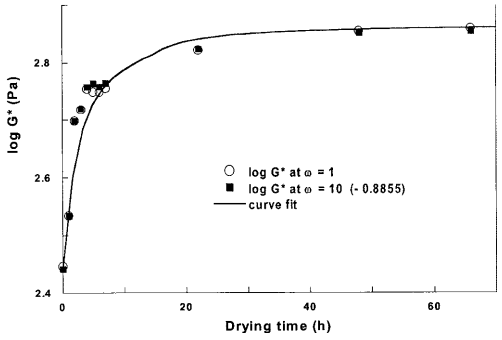

Fig. 1 Complex shear modulus at 1 and 10 rad/s vs drying time under vacuum at 80 °C. The line shows curve fit to log $G^* = a_0 + a_1 \exp\{-a_2/t\}$, with the fitting parameters $a_o = 2.444 \pm 0.014$, $a_1 = 0.427 \pm 0.014$, and $a_2 = 1.400 \pm 0.105$. The standard deviation of data and the correlation coefficient squared are, respectively, $\sigma = 0.020$ and $r^2 = 0.99995$. Thus, 48 h drying reaches log G* level 0.4% below the value expected for infinite drying time

samples listed in Table 1 were tested. As shown in Fig. 2, the extrusion introduced only a minor change in the flow behavior of neat PA, but it did reduce G' and G'' of the PNC by 74 and 20%, respectively.

The time sweep results were fitted to a second-order polynomial, with t being the sweep time (in seconds):

$$G' = G'_o + G'_1 t + G'_2 t^2;\ dG'/dt = G'_1 + 2G'_2 t$$
$$G'' = G''_o + G''_1 t + G''_2 t^2;\ dG''/dt = G''_1 + 2G''_2 t \quad (1)$$

The fitting parameters and correlation coefficient (r) are listed in Table 1 where the five upper compositions were extruded prior to testing and the two at the bottom were tested "as received". After testing the specimens did not show signs of oxidative reactions – they remained off-white. Thus, the most likely reason for the increase of the shear moduli is polycondensation. Even after a 1-h test the rate show but a small decrease. As to be expected, the effect on G' is stronger than that on G''. In 1 h G' and G'' values increased by up to 450 and 95%, respectively.

To observe the effect of organoclay content on the time-dependent variation of dynamic moduli the rates of change at t = 0 and 1000 s were computed from Eq. (1) (see Fig. 3). Their compositional dependence was described using a polynomial:

$$dG'/dt = (G')'_o + (G')'_1 w + (G')'_2 w^2$$
$$dG''/dt = (G'')'_o + (G'')'_1 w + (G'')'_2 w^2 \quad (2)$$

Numerical values of Eq. (2) parameters and the correlation coefficient, r, are listed in Table 2.

Strain sweeps

The strain sweeps were conducted in the range $\gamma = 0$–100% at T = 240 °C and $\omega = 6.28$ rad/s for about

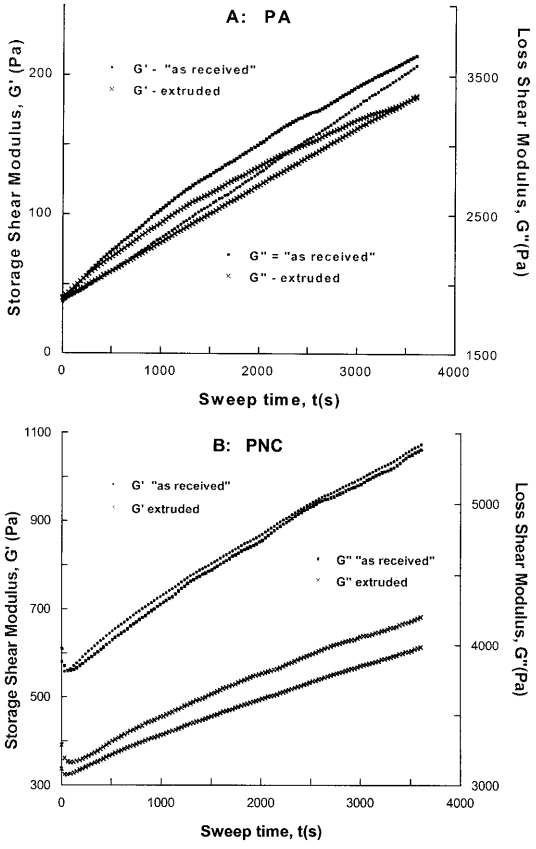

Fig. 2A, B Shear moduli at $\omega = 6.28$ rad/s and strain of $\gamma = 10\%$ vs sweep time at 240 °C for "as received" and extruded: **A** PA; **B** PNC. Note the large enhancement of the storage modulus upon addition of clay

t ≤ 600 s. At this relatively high frequency the compositions containing 100, 75, and 50% of PNC showed viscoelastic non-linearity at strains of $\gamma \geq 12$–20%.

The strain effects on G' and G'' were described using KBKZ-type non-linearity expression. As shown in Fig. 4, the shear moduli are well approximated by

$$G''(\gamma) = G''_o/[1 + G''_1 \gamma_f^2 - G''_2 \gamma_f^3];\ \text{strain fraction: } \gamma_f = \gamma/100 \quad (3)$$

The parameters of Eq. (3) for G' and G'' are listed in Table 3, along with the measure of the non-linear least squares fitting statistics (σ = standard deviation; r^2 = correlation coefficient squared; CD = coefficient of determination).

In Fig. 5 the calculated constant strain ($\gamma = 0$ and 50%) values of G' and G'' at $\omega = 6.28$ rad/s are plotted vs PNC content. Evidently, for w ≤ 50 wt% the strain effects are quite small. Even for neat PNC at $\gamma = 50\%$ the reduction of G' and G'' is only by, respectively, 15 and 7.5%.

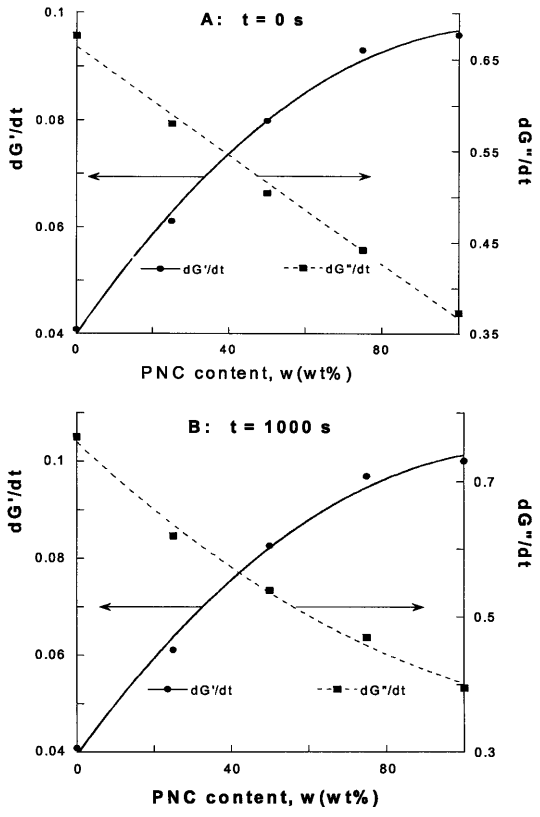

Fig. 3A, B Concentration dependence of the rate of G′ and G″ change during the time sweep (see text): **A** values extrapolated to the initial moment (t = 0); **B** values interpolated to the test time t = 1000 s. *Lines* represent least-squares fit to Eq. (2), with parameters listed in Table 2

Frequency sweeps – loss modulus

Frequency sweeps were conducted at T = 240 °C, strains $\gamma = 10$ and 40%, in two directions: $\omega = 0.1$–100 and $\omega = 100$–0.1 rad/s as well as $\omega = 10$–0.1 rad/s. As an example, results for extruded PNC are shown in Fig. 6. At 10% strain the data do not depend on the scan direction, but at $\gamma = 40\%$ most do.

At $\gamma = 40\%$ only for PA and the mixture containing 25 wt% PNC the moduli G' and G'' are the same for the two scan directions. Thus, scanning by either increasing or decreasing frequency, or scanning in the same direction but starting from different frequency, produce different rheological response – nearly twice as large for G' as for G''. The differences were found to increase linearly with organoclay content. Evidently the internal structure of PA-6 containing >0.5 wt% organoclay is easily modified by strain and frequency, resulting in different rheological responses. These unexpected shear history effects were well reproduced by two instrument operators who used two rheometers and a variety of specimens. Note that the experimental error of the measurements is ±2%.

Table 2 Polynomial fit parameters for the rate of change at time t = 0 and 1000 s (see Eq. 2)

Parameter	Value at t = 0 s	Value at t = 1000 s
$(G')'_0$	0.0399	0.03952
$(G')'_1$	0.00103	0.001091
$(G')'_2$	-4.640×10^{-6}	-4.718×10^{-6}
r	0.9981	0.0069
$(G'')'_0$	0.6632	0.7574
$(G'')'_1$	−0.0297	−0.005310
$(G'')'_2$	0	1.7521×10^{-5}
r	0.9966	0.9968

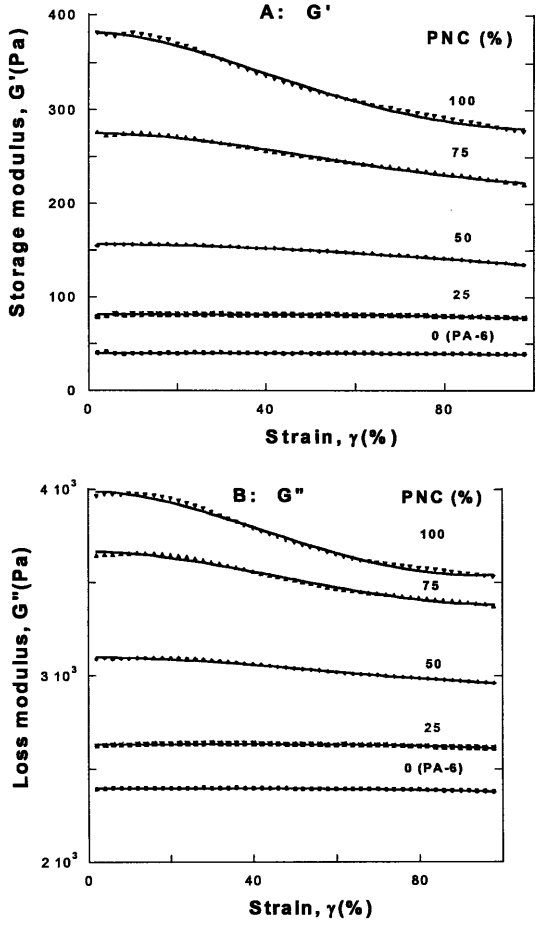

Fig. 4A, B Strain sweep of: **A** G′; **B** G″ at T = 240 °C and $\omega = 6.28$ rad/s for extruded PA/PNC mixtures – *points* experimental, *lines* computed using non-linear least squares fit to Eq. (3). The fitting parameters are listed in Table 3

To analyze the frequency dependence of G'' the data at $\gamma = 10\%$ scanned in both directions and those at 40% scanned from 100 to 0.1 rad/s were used. The data (corrected for the time effects) were fitted to the Krieger-

Table 3 Strain effects on G′ and G″ for PA-6/PNC at T = 240 °C and ω = 6.28 rad/s; see Eq. (3)

Parameter	PA-6	25% PNC	50% PNC	75% PNC	100% PNC
G'_0	40.30 ± 0.10	81.49 ± 0.16	156.69 ± 0.12	275.48 ± 0.36	381.54 ± 0.77
G'_1	–0.041 ± 0.026	–0.059 ± 0.020	0.1699 ± 0.009	0.5367 ± 0.015	1.0637 ± 0.026
G'_2	–0.0725 ± 0.0267	–0.1079 ± 0.0211	0.0032 ± 0.0092	0.2990 ± 0.0163	0.7046 ± 0.0281
σ	*0.36262*	*0.57162*	*0.4270*	*1.1914*	*2.4496*
r^2	*0.999923*	*0.999953*	*0.999992*	*0.999978*	*0.99995*
CD	*0.51158*	*0.801510*	*0.99641*	*0.99566*	*0.99534*
G''_0	1903.2 ± 0.7	2134.3 ± 0.8	2603.3 ± 1.3	3169.4 ± 2.6	3490.1 ± 3.7
G''_1	–0.067 ± 0.003	–0.013 ± 0.004	0.1296 ± 0.005	0.3002 ± 0.009	0.504 ± 0.012
$1000 \times G''_2$	–0.565 ± 0.037	–0.238 ± 0.041	0.720 ± 0.053	2.014 ± 0.090	3.59 ± 0.12
σ	*2.4293*	*2.9542*	*4.4703*	*8.6453*	*12.316*
r^2	*0.999998*	*0.999998*	*0.999997*	*0.99999*	*0.99999*
CD	*0.93973*	*0.84360*	*0.99147*	*0.99293*	*0.99437*

Daugherty type dependence, written for the dynamic flow as Utracki (1984):

$$\eta' \equiv G''_{corr}/\omega = \eta_o[1 + G''/G\eta]^{-m_1};$$
$$\psi \equiv G'_{corr}/\omega^2 = \psi_o\left[1 + (G''/G_\psi)^2\right]^{-m_2} \quad (4)$$

Equation (4) was derived for linear viscoelastic, pseudo-plastic systems and hence it is unable to describe the yield stress. For PA all data points follow Eq. (4), but for the other compositions only data at $\omega > \omega_c \cong 1.4 \pm 0.2$ rad/s may be used. The parameters of Eq. (4) are listed in Table 4 and plotted in Fig. 7.

The frequency dependence of the dynamic viscosity (η') is shown in Fig. 8, along with the dependence given by Eq. (4). The most interesting observation is the deviation from the limiting linear viscoelastic behavior at a characteristic frequency, ω_c. The effect is associated with a change of the specimen structure. It is particularly strong for PNC content w ≥ 50 wt%. As expected, the change is more evident at strain of 40% than of 10%.

Intrinsic viscosity and the aspect ratio

The zero-shear viscosities (η_o) from Table 4 can be plotted as relative viscosity (η_r) vs clay volume fraction (ϕ). The data for the five concentrations of PNC (see Fig. 9) show a typical trend for suspensions of anisometric particles. Considering the low clay concentration ($\phi \le 0.0064$) the data were fitted to the second-order, Einstein-type equation:

$$\eta_r = \eta'_o/\eta'_{o,PA} = 1 + [\eta]\phi + k([\eta]\phi)^2 \quad (5)$$

The least-squares fit gives values for the intrinsic viscosity: $[\eta] = 105.5 \pm 22.5$ and for the interaction constant $k = 0.52 \pm 0.058$, with the measures of fit $\sigma = 0.0674$ and $r^2 = 0.9983$.

As was already predicted by Simha (1940), the intrinsic viscosity depends on the aspect ratio, p (Utracki 1989):

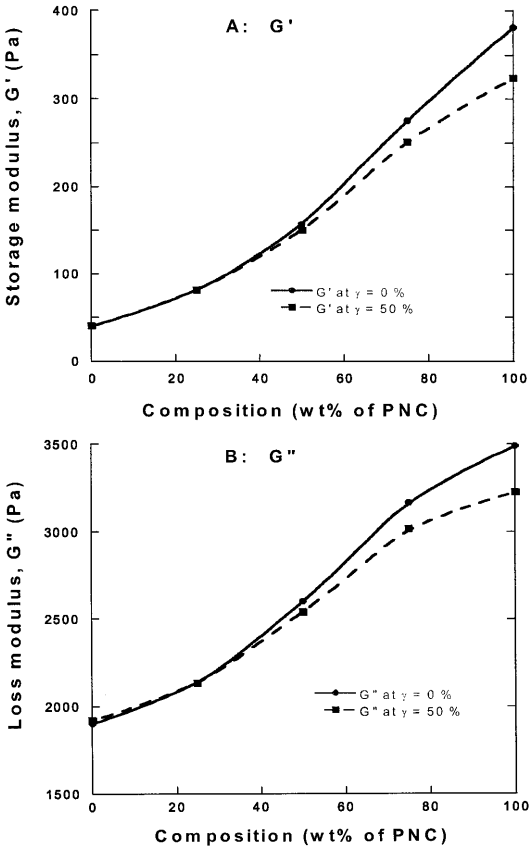

Fig. 5A, B Plot of: **A** storage; **B** loss shear moduli at T = 240 °C, $\omega = 6.28$ rad/s, and $\gamma = 0$ or 50% for extruded PA/PNC mixtures. *The lines* are only to guide the eye

$$[\eta]_{disks} = 2.5 + a(1 - p^b) \quad (6)$$

For disks (or platelets) the parameters in Eq. (6) are $a = 0.025 \pm 0.004$, $b = 1.47 \pm 0.03$, with $\sigma = 0.6214$ and $r^2 = 0.9998$. This dependence is shown in Fig. 10, where the determined value of [η] yields a modest aspect ratio

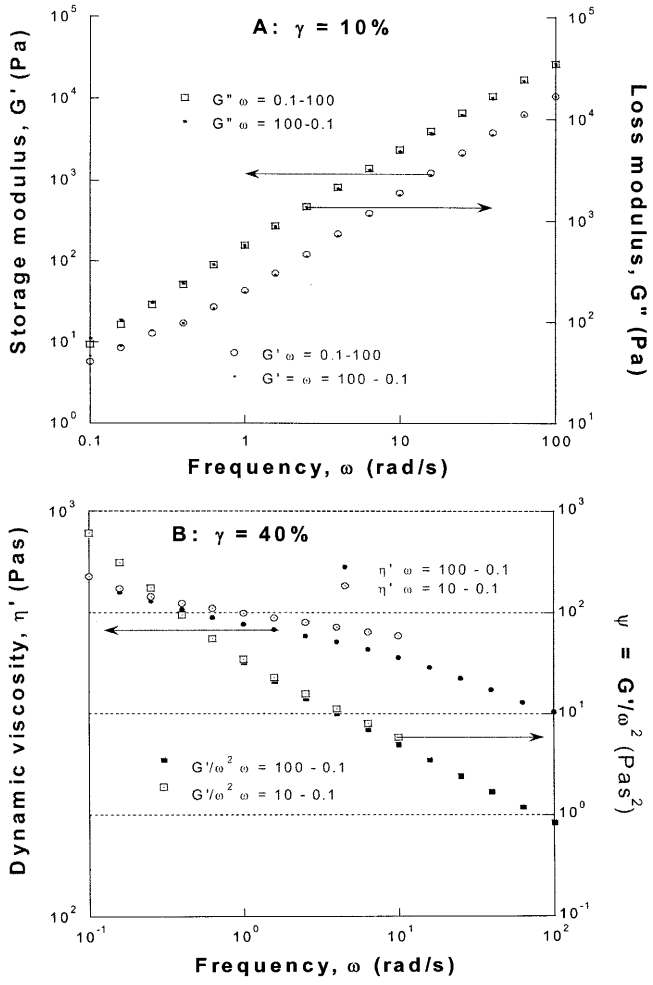

Fig. 6A, B Frequency scans for extruded PNC at 240 °C: **A** at $\gamma = 10\%$ from 0.1 to 100 and from 100 to 0.1 rad/s (different specimens); **B** at $\gamma = 40\%$ from 100 to 0.1 and from 10 to 0.1 rad/s (different specimens)

for the MMT, $p = 287 \pm 9$; hence the maximum packing volume fraction of these clay platelets is $\phi_{m,plate} = (3/2p)\phi_{m,sphere} \cong 0.00324$. Thus, theory predicts that up to a clay content of $w_m \cong 1.01$ wt% (or ca. 50% PNC in the mixture with PA) the platelets are able to rotate freely.

To judge whether the calculated aspect ratio is realistic, the permeability data for PNC were used. Specifications for the PA and PNC resins list the moisture permeability as 203 and 106 g/(m^2 day), respectively (Ube Industries 2000). The relative permeability coefficient (P_r) can be related to p through the tortuosity argument as

$$P_r = [1 + p\phi/2]^{-1} \tag{7}$$

Substituting $P_r = 0.522$ and $\phi = 0.0064$ into Eq. (7) gives $p = 286$, well within the range of values computed from the dynamic viscosities.

Apparent yield stress

A deviation from the limiting linear viscoelastic behavior is observed (see Fig. 8) at low frequencies. The increasing value of G'' as the frequency is reduced below $\omega_c = 1.4 \pm 0.2$ rad/s is related to the formation of a 3-D structure that leads to a yield stress. From the data in Fig. 8 one can extract the yield function defined as: $Y \equiv \eta'_{exp}/\eta'_{lin} = G''_{exp}/G''_{lin}$, from which the apparent yield stress can be calculated as: $\sigma_y(\omega) = (Y-1)G''_{lin}$. The plot of Y vs ω is shown in Fig. 11.

Assuming a dynamic cluster formation of interacting particles in a multiphase system an expression for the dynamic yield stress was derived (Utracki 1989):

$$\sigma_y(\omega) = \sigma_y^o\left[1 - \exp\{-\tau_y\omega\}\right] \tag{8}$$

where σ_y^o is a measure of the interacting strength, τ_y is the relaxation time of the dynamic cluster, and the exponent u is a measure of the cluster polydispersity.

It was found that for the PA/PNC mixtures the yield stress $\sigma_y = \sigma_y(\omega)$ follows Eq .(8) with constant value of $\tau_y = 0.59 \pm 0.03$ s and $u \cong 1$. The values of the interacting strength parameter, σ_y^o, were found to increase linearly with PNC content. The solid-like structure formation starts at about 20 wt% PNC reaching the maximum value of $\sigma_y^o = 23$ Pa for the neat PNC. It is noteworthy that the onset of the yield stress takes place at the MMT concentration about 2.5 times lower than that calculated for the platelet maximum packing fraction. Thus, the 3-D structure formation in end-tethered systems seems to be facilitated by the presence of macromolecules attached to the layered silicate surface.

Since at $\omega < 1$ rad/s G' is within the experimental error, its yield stress was not evaluated.

Frequency sweeps – storage modulus

According to Doi and Edwards (1978), a plot of log G' vs log G'' for "well behaving" liquids should follow a straight line with the slope of 2:

$$\ln G' = 2 \cdot \ln G'' + \ln(6M_\epsilon/5\rho RT) \tag{9}$$

Figure 12 show the log G'/G'' vs log G'' dependence for all PA/PNC compositions, frequencies, and strains. Excepting a small difference in values for PNC, the data for 10 and 40% strains superpose. The observed deviation from the expected linearity originates from the inter-particle interactions that more strongly affect the storage than the loss modulus. In simple words, addition of tethered clay particles to PA matrix results in higher values for the stored energy than expected from the second-order fluid.

In Fig. 13 the data measured at $\gamma = 10$ and 40% are plotted as the stored energy parameter, $\psi \equiv G'/\omega^2$ vs ω. The lines were computed by fitting these data to Eq. (4)

Table 4 Frequency effects on G″ and G′ for PA-6/PNC mixtures at γ = 10 and 40%

Parameter	PA-6	25% PNC	50% PNC	75%PNC	100% PNC
1. $\eta' = G''/\omega$ at T = 240 °C and γ = 10%					
η_0	303.3 ± 0.6	333.5 ± 0.6	443.1 ± 1.4	495.1 ± 2.1	542.4 ± 3.1
m_1	0.1333 ± 0.0037	0.1335 ± 0.0112	0.1228 ± 0.0039	0.1356 ± 0.0041	0.1503 ± 0.0037
log G_η	1.870 ± 0.0019	1.4547 ± 0.0049	0.8321 ± 0.0136	0.5488 ± 0.0321	0.4781 ± 0.0372
σ	*0.000275*	*0.00155*	*0.00148*	*0.00215*	*0.00188*
r^2	*0.999 999 0*	*0.999 999 7*	*0.999 999 8*	*0.999 999 5*	*0.999 999 6*
CD	*0.969 777*	*0.996 717*	*0.999 618*	*0.999 078*	*0.999 441*
2. $\eta' = G''/\omega$ at T = 240 °C and γ = 40%					
η_0	302 ± 1	334 ± 3	434 ± 4	495 ± 10	543 ± 18
m_1	0.121 ± 0.251	0.1344 ± 0.0567	0.124 ± 0.033	0.136 ± 0.046	0.150 ± 0.056
log G_η	1.8404 ± 0.0019	1.3947 ± 0.0198	0.8321 ± 0.0136	0.5411 ± 0.0560	0.4672 ± 0.0416
σ	*0.00137*	*0.00161*	*0.00159*	*0.00230*	*0.00203*
r^2	*0.999 999 8*	*0.999 999 7*	*0.999 999 8*	*0.999 999 5*	*0.999 999 6*
CD	*0.993 585*	*0.996 715*	*0.999 231*	*0.999 078*	*0.999 441*
3. $\psi = G'/\omega^2$ at T = 240 °C and γ = 10 and 40%					
log (ψ_0)	0.00027 ± 0.00323	0.3893 ± 0.0122	0.912 ± 0.024	1.494 ± 0.053	1.864 ± 0.069
m_2	0.2277 ± 0.0096	0.2577 ± 0.0103	0.702 ± 0.030	0.752 ± 0.025	0.816 ± 0.026
log G_ψ	1.2471 ± 0.0298	0.6876 ± 0.0532	0.421 ± 0.085	–0.143 ± 0. 0.118	–0.3892 ± 0.134
σ	0.00759	0.0209	0.025106	0.0282760	0.036663
r^2	0.99816	0.99423	0.997888	0.9990709	0.998994
CD	0.996539	0.9928	0.99511	0.996069	0.995322

with values of the fitting parameters listed in Table 4. Evidently, $\psi = G'/\omega^2$ follows Eq. (4) rather well. However, the fit was attempted only for higher frequencies, as for $\omega \leq 1$ rad/s the values of G' are within experimental error. It is noteworthy that (as discussed for G'') a 3-D structure was noted only at $\omega < \omega_{crit}$; thus G' is free from the effects associated with the yield stress.

The concentration dependence of the principal parameters of Eq. (4), η_0 and G_η or ψ_0 and G_ψ may be approximated by the second-order polynomial in semi-logarithmic plot (see Fig. 7):

$$\log \eta_o = a_0 + a_1 w + a_2 w^2 \tag{10}$$

Numerical values of the a_i parameters and the measures of the goodness of fit are listed in Table 5. In these calculations the composition was expressed as wt% of PNC. Since in PNC there is 1.6 wt% clay, its influence on the dynamic flow is remarkable.

Addition of clay platelets has a stronger effect on ψ than on η'. Thus, for PA the ratio η_o/ψ_o is about 300, whereas for PNC it is about 8. The concentration dependence of ψ_o is about five times stronger than that of η_o. There is also significant difference in the power-law exponent behavior for η' and ψ – for the former function $n = 0.84 \pm 0.07$, whereas for the latter n is a decreasing function of the PNC content.

Theory

For the incompressible, linear viscoelastic liquid there is an interrelation between G′ and G″ through the relaxation spectrum, H(λ):

$$\frac{G'}{\omega^2} = \int_0^\infty \frac{\lambda H(\lambda) d\lambda}{1 + (\omega\lambda)^2}$$
$$\frac{G'}{\omega} = \int_0^\infty \frac{H(\lambda) d\lambda}{1 + (\omega\lambda)^2} \tag{11}$$

Since these functions are valid in the whole range of the relaxation times, they are also valid within narrow ranges inside this interval, say from $\lambda = t$ to $(t + \Delta)$, when Eq. (11) can be written in terms of averages (for the interval) as:

$$\left(\frac{G'}{\omega^2}\right) = \Delta \frac{\xi H(\xi)}{1 + (\omega\xi)^2} = \xi(G'/\omega);\ t \leq \xi \leq t + \Delta \tag{12}$$

The mean value theorem only requires that the integrals be continuous and the interval Δ small. Thus, one can expect that the proportionality between the two components of the dynamic function should be preserved in the full range of the relaxation time and frequency. For Maxwell fluid Eq. (12) gives

$$\left(\frac{G'}{\omega^2}\right) = \lambda\left(\frac{G''}{\omega}\right) \quad \text{or} \quad \psi(\omega) = \lambda\eta'(\omega) \tag{13}$$

where λ is the main relaxation time. Thus, the simple Maxwell model represents the flow behavior for fluids in which the ratio of parameters in Eq. (4) $m_2/m_1 = 2$. As the data in Table 4 show, only for PA-6 and the 25% PNC mixture is this condition approximately observed – for the other systems $m_2/m_1 \cong 5.5$; hence these systems are rheologically complex.

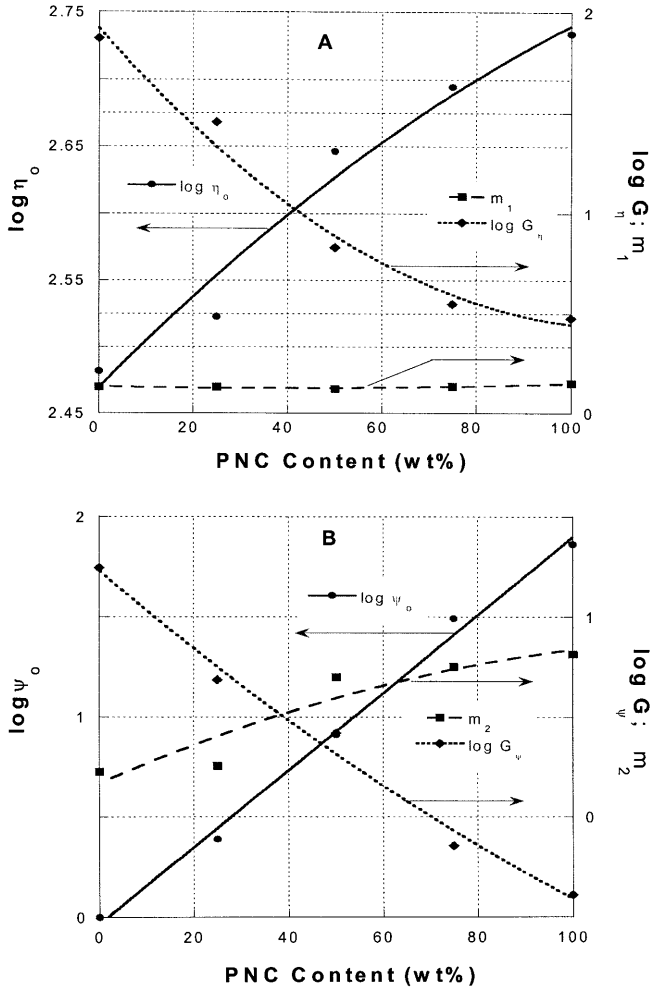

Fig. 7 Composition dependence of Eq. (4) parameters for PA/PNC mixtures at 240 °C: **A** G″ data at $\gamma = 40\%$; **B** G′ data at $\gamma = 10$ and 40%. *The lines* represent second order polynomial fit with parameters listed in Table 5

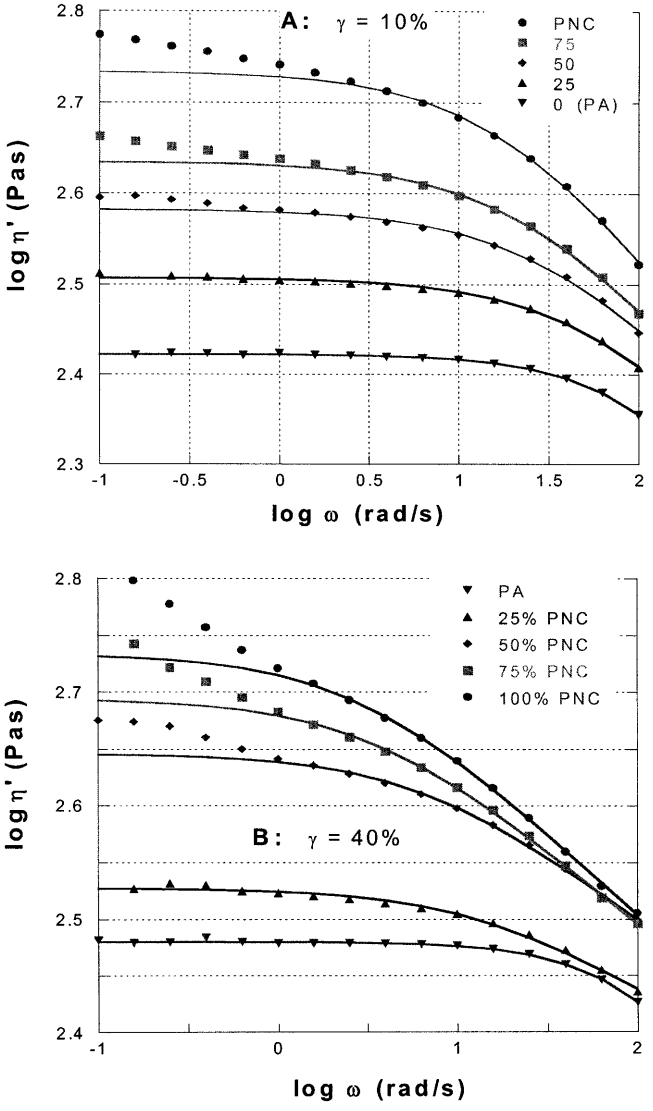

Fig. 8 Frequency-dependent dynamic viscosity for PA/PNC mixtures at T = 240 °C and at strain: **A** $\gamma = 10\%$; **B** $\gamma = 40\%$. *Points* are experimental, *lines* computed from Eq. (4) with parameters listed in Table 4

Discussion

Dynamic melt flow at T = 240 °C of PA-6 and nanocomposite resins based on it was investigated. The specimens were well dried before testing. The tests under a blanket of dry nitrogen were accompanied by the time-dependent increase of PA-6 molecular weight that had to be taken into account. The PNCs belong to the category of end-tethered nanocomposites, reported to show a complex rheological behavior (Krishnamoorti and Giannelis 1997; Hoffmann et al. 2000a, 2000b; Ren et al. 2000; Solomon et al. 2001; Galgali et al. 2001).

The rheological properties of polyamides are known to depend on the measurement time. For example, Khanna et al. (1996) reported that PA-6 viscosity increased during the melt flow measurements by a factor of 2–5. This reversible change is related to the variation of the moisture content and associated with changes of molecular weight, i.e., to polycondensation.

The time-dependence of the shear moduli was found independent of strain ($\gamma = 10$ or 40%) and slightly dependent on the direction of frequency change. The latter, secondary in magnitude effect, was observed during the frequency sweeps, where the rate of moduli increase was different for sweeps from 0.1 to 100 rad/s than that from 100 to 0.1 rad/s. The data were fitted to a second-order polynomial with parameters listed in Table 1. From these the rates of change for G' and G'' at $t = 0$ and $t = 1000$ s were calculated.

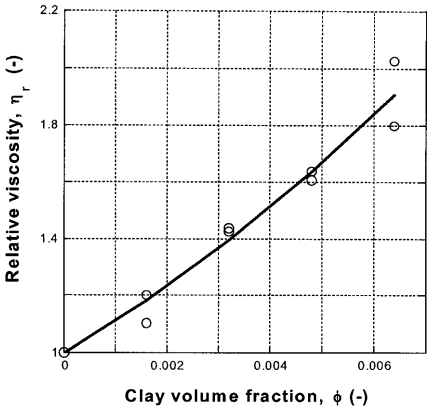

Fig. 9 Zero-shear relative viscosity at T = 240 °C, $\gamma = 10$ and 40% as a function of clay volume fraction. *Points* – experimental, *line* – least-squares fit to Eq. (5)

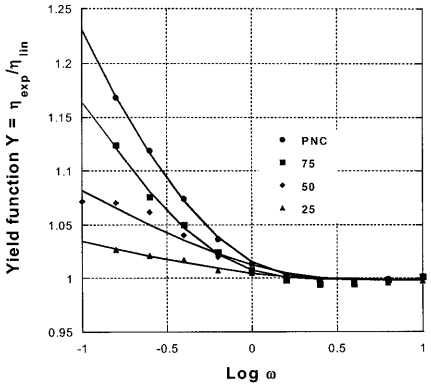

Fig. 11 Frequency dependence of the yield stress function $Y \equiv \eta'_{exp}/\eta'_{lin} = G''_{exp}/G''_{lin}$ for PA/PNC mixtures (containing 25–100% of PNC), at T = 240 °C. *Lines* computed from Eq. (8) express the yield stress as $\sigma_y(\omega) = (Y - 1)G''_{lin}$

As shown in Fig. 3, the rates are positive, but increasing the organoclay content caused a decrease of dG''/dt and increase of dG'/dt. In other words, in respect to PA-6, addition of organoclay slows down the time-induced increase of G'', but it accelerates that of G'. This dual effect may be caused by two parallel mechanisms that increase both G' and G'': (1) polycondensation and (2) exfoliation. Evidently, addition of organoclay slows the polycondensation, most likely caused by the presence of residual low molecular weight amines (introduced during the intercalation and/or polymerization steps). There is also another mechanism possible, but before discussing it a PNC structure should be considered.

Composition and properties of natural montmorillonite vary with geographical location and local strata. However, an idealized Na-MMT unit cell can be written as

Triple layer sandwich of two silica tetrahedron sheets and a central octahedral sheet with 0.67 negative charge per unit cell

$$[Al_{3.33}Mg_{0.67}]^{-(0.67)}\ Si_8O_{20}(OH)_4$$

$$\Downarrow$$

Aqueous interlammelar layer containing 0.67 Na^+ cations per unit cell

$$(n \times H_2O)\ Na^+_{0.67}$$

Thus, the molecular weight of unit cell is $M_u = 734 +$ water and the cation exchange capacity of idealized MMT is CEC = 0.915 meq/g, with Na^+ spaced ca. 1.2 nm apart.

Postulated mechanism for PNC preparation is Na^+ exchange for onium ion (12-aminolauric acid) that leads to end-tethering the PA-6 chains. Since the molecular

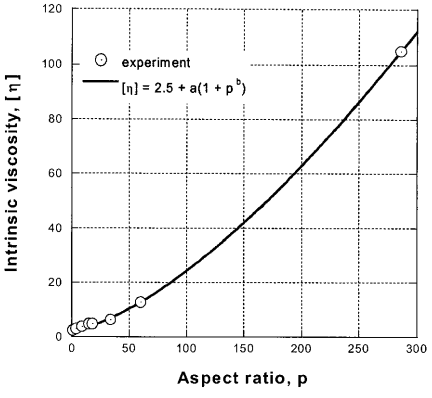

Fig. 10 General dependence of platelets intrinsic viscosity vs aspect ratio (Utracki 1989). The *solid line* was computed from Eq. (6) (see text)

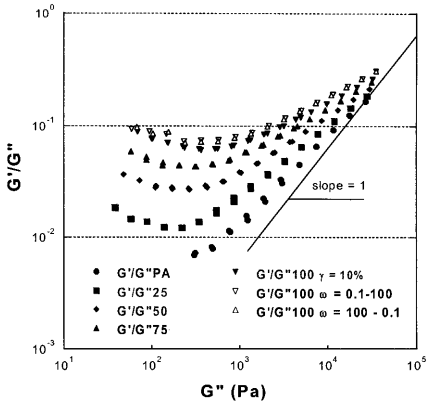

Fig. 12 Inverse loss tangent vs loss modulus for PA/PNC mixtures at T = 240 °C and $\omega = 0.1$–100 rad/s. *Solid symbols* represent data at strain $\gamma = 10\%$ and *open symbols* (PNC, in two scanning directions) at $\gamma = 40\%$. For the frequency-independent entanglement network Eq. (9) predicts slope = 1

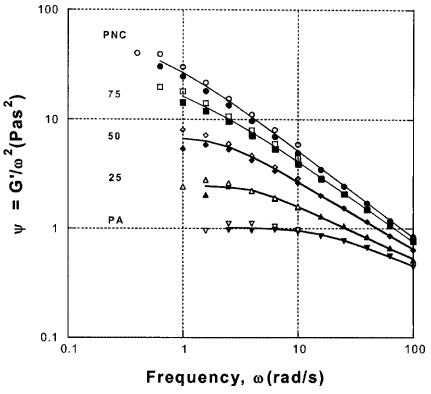

Fig. 13 Stored energy parameter, $\psi = G'/\omega^2$, vs frequency, ω, for PA/PNC mixtures at T = 240 °C. *Open and solid symbols* represent data at 10 and 40% strain, respectively. The *lines* were computed from Eq. (4). Fitting parameters are listed in Table 4

Table 5 Parameters of Eq. 10 for η_o, G_η and m_1 as well as for ψ_0, G_ψ and m_2. System: PA/PNC mixtures at T = 240°C and indicated strain

Parameter	a_o	a_1	a_2	r^2
log η_0 (Pas); γ = 40%	2.4696	0.00360	−8.96e-06	0.9837
log G_η (Pa); γ = 40%	1.9205	−0.02647	0.0001172	0.9917
m_1; γ = 40%	0.1354	−0.00046	6.007e-06	0.9180
log ψ_0 (Pas^2); γ = 10 and 40%	−0.0315	0.01909	2.427e-06	0.9973
log G_ψ (Pa); γ = 10 and 40%	1.2324	−0.02017	3.762e-05	0.9939
m_2; γ = 10 and 40%	0.1697	0.01043	−3.745e-05	0.9411

weight of PA-6 is $M_n = 22$ kg/mol, the resulting clay content of the fully grafted "hairy clay plates" (HCP) should be 4.74 wt%. Since the clay platelets are 0.96 nm thick and their aspect ratio is p = 287, each plate has about 140,000 end-tethered macromolecules, i.e., $M_n \cong 3 \times 10^6$ kg/mol of a single HCP. Thus, polycondensation that involves every Na^+ on the Na-MMT surface results in formation of an entity that resembles a star-branched macromolecule of a very high molecular weight. Near the clay surface the macromolecules are crowded and forced to stretch out. Since PNC used in this work has 1.6 wt% of clay, it would comprise 34% HCP and 66% free PA-6 macromolecules.

The above calculations assumed that every clay plate and every cation on its surface is available for the reaction. This may not be correct, considering that initially there are hundreds of platelets in each tightly packed stack. The intercalation, polymerization, and post-polymerization shearing usually reduce the size of the stack to few platelets, which on average may have fewer tethered macromolecules. Furthermore, during the rheological tests the short stacks may progressively exfoliate, the free HCPs having fewer end-tethered chains. For the sake of argument, let us assume that in PNC only every third Na^+ ion is replaced by end-tethered macromolecule; hence there are no free PA molecules present.

In the absence of oxygen and moisture, molten PA is in the state of dynamic chemical equilibrium, where two macromolecules react, freeing one molecule of H_2O, which then attacks the PA chain at random. In the case of PA-6, each free macromolecule has one $-NH_2$ and one −COOH group at the chain ends. This evidently is not the case for the end-tethered ones – for them only the –COOH group is available. When PA is mixed with PNC the chemical randomization process is non-symmetric – fewer bonds can be broken in the macromolecule attached to the clay platelet than in the one that is not attached. Since polycondensation polymers are polydispersed, one would expect the free chains to have lower molecular weight. As a result, addition of PNC should, as observed, accelerate the increase of dG′/dt and decrease that of dG″/dt.

This description of PNC structure also concords with the observation that ratio of energy stored-to-dissipated changes from $G'/G'' \cong 0.01$ (for PA and 25% PNC) to about 0.1 for PNC (see Fig. 12). In short, addition of HCP causes a more rapid increase of the stored than dissipated energy, increasing the G′/G″ ratio.

As shown in Fig. 8, the clay-containing resins have bi-modal relaxation time dependence, separated by the critical frequency $\omega_c \cong 1.4 \pm 0.2$ rad/s. Considering that the period of a platelet rotation is given by $t_{rotation} = 2\pi(p + 1/p)/\dot{\gamma}$ it is evident that presence of the critical frequency is not related to clay platelets, but rather to a PA-6 network.

At $\omega > \omega_c$ the flow may be represented by Eq. (4), derived for pseudoplastic systems. However, within this frequency region again one should consider separately the moderate and the high frequency domains. At the moderate frequencies there are strong clay concentration effects on η_o, ψ_o, G_η, and G_ψ (see Fig. 7). For example, the characteristic stress parameter of Eq. (4) are $G_\eta = 71$, 25, 6.7, 3.6, and 2.9 for, respectively, PA, 25%, 50%, 75%, and 100% PNC. A similar tendency is observed for G_ψ, whereas η_o and ψ_o increase with PNC concentration. However, at the highest frequencies the flow of all compositions follows the power-law dependence with the same exponent: $n = 0.84 \pm 0.07$ – evidently here the flow is controlled by PA matrix.

The frequency sweeps were carried out at two strain levels, $\gamma = 10$ and 40% within the frequency range, $\omega = 0.1$–100 rad/s. Depending on the strain and frequency, linear and nonlinear rheological behavior was observed. PA-6 resin showed linear viscoelastic behavior in the full range of frequency at both levels of strain. The mixtures of PA with PNC at strain $\gamma = 10\%$ showed

linear behavior within a limited range of frequency, $\omega > \omega_c = 1.4 \pm 0.2$ rad/s, whereas at $\gamma = 40\%$ only PA and 25% PNC showed such behavior.

For all samples, the strain dependence of the storage and loss moduli follows the KBKZ-type dependence, decreasing with strain. However, the reduction is relatively modest, e.g., for PNC (at $\omega = 6.28$ rad/s and $\gamma = 50\%$) G″ and G′ decreased, respectively, by 7.5% and 15%.

Two types of flow non-linearity were observed:

1. At low frequency, $\omega \leq \omega_c = 1.4 \pm 0.2$ rad/s, there was evidence of an apparent yield stress in samples containing w ≥ 1 wt% of organoclay. This transient, solid-like behavior has been associated with existence of a 3-D structure. Analysis of the dynamic yield stress indicates that its magnitude varies linearly with clay concentration, while the cluster relaxation time remains constant, $\tau_y = 0.59 \pm 0.03$ s. Extrapolation of the observed data makes it possible to estimate that the onset of the 3-D structure should take place for PA-6 mixtures with ca. 20 wt% PNC, i.e., for nanocomposite containing 0.4 wt% of organoclay. Formation of these 3-D structures is critically sensitive to the frequency – independently of the clay content they seem to break at $\omega > \omega_c = 1.4 \pm 0.2$ rad/s.
2. At $\omega > \omega_c$ the 3-D structure is apparently broken, but the melt is far from homogenous. Within this frequency region the magnitude of the shear moduli depends not only on strain and frequency but also on the history of deformation. Thus, at strain $\gamma = 10\%$, the flow curves were independent of the direction of the frequency scan and they followed a Krieger-Daugherty type of dependence. However, at $\gamma = 40\%$ the samples containing w > 25 wt% of PNC showed different values of the shear moduli depending on the initial frequency and/or the direction of the frequency scan. There are two possible mechanisms that may explain the behavior: (1) higher orientation of clay platelets at higher frequency, and (2) reduction of interparticle interactions. Within the power-law flow region the power exponent is constant and the flow depends mainly on the matrix; hence here the giant HCPs are expected to be fully oriented in the flow direction. This postulate is in agreement with observation that the critical rate of shear for platelets orientation in PEG solution $\dot{\gamma}_{critical} = 30\ (1/s)$ (Schmidt et al. 2000) as well as the conclusions drawn by Ren et al. (2000) that large-amplitude oscillations are able to orient clay structures and increase the liquid-like NC behavior.

It may be concluded that at relatively low loading of the end-tethered clay platelets, say above 20 wt% PNC, the HCP form interacting aggregates. Suspensions of these anisometric, grafted particles may undergo gelation and network formation at $\omega < \omega_c$. These structures are broken at $\omega > \omega_c$ and initially the melt flows as a pseudoplastic suspension with unoriented HCP. However, at the higher still frequencies, the platelets become oriented and the flow starts to be dominated by the matrix. It is the orientational effect that causes the rheological response to vary not only with the imposed variables, but also with the strain history – once the orientation is imposed by higher strain and frequency, its randomization take time. When the frequency (at given strain) is reduced, the platelets orientation randomizes and the values of G′ and G″ tend toward a stable value –the PNC melt behaves like a classical suspension.

Applying the Krieger-Daugherty equation to this region one is able to determine η_o, then $[\eta]$, from which the aspect ratio of the exfoliated clay platelets can be calculated. The value of the latter, $p = 287 \pm 9$, agrees well with that computed from the permeability data. For freely rotating disks, the ratio of encompassed to the actual volume is 2p/3, and the maximum packing volume of individual, free rotating platelets is $\phi_{m,plate} = (3/2p)\phi_{m,sphere} \cong 0.00324 = 1.01\ wt\%$. These calculations do not take into account the presence of the end-tethered PA-6 chains; hence one must expect that in the PA/PNC mixtures the hydrodynamic interactions will occur at lower concentration. Indeed, there is evidence of interparticle interactions already for 50 wt% PNC, i.e., for a mixture containing 0.8 wt% of clay. However, the free rotation of platelets takes place in 25 PNC sample, containing 0.4 wt% of clay.

Conclusions

1. At constant T, γ, and ω the time sweeps resulted in significant increases of the shear moduli, G' and G'', caused by a progressive polycondensation of PA-6 and possibly in exfoliation of organoclay. The rate dG''/dt decreased with organoclay content, whereas dG'/dt increased.
2. At $\gamma = 10\%$ and at $\omega > 1$ rad/s all samples showed linear viscoelastic behavior, but at $\gamma = 40\%$ only PA and 25 PNC samples.
3. Compositions containing ≥50% PNC exhibited two types of viscoelastic non-linearity. At low frequencies, $\omega \leq \omega_c = 1.4 \pm 0.2$ rad/s, a yield stress provided evidence of a 3-D structure. At higher frequencies, $\omega > \omega_c$, G' and G'' were sensitive to shear history, e.g., starting at higher strain or frequency resulted in lower values of G' and G'' – the effect was reversible. Such a transient non-linearity is consistent with strain and frequency dependent orientation of anisometric clay particles.

4. At high frequency the dynamic viscosity, $\eta' = G''/\omega$, showed a constant power-law exponent for all (but PA-6) samples, $n = 0.84 \pm 0.07$, indicating matrix disentanglement related mechanism of flow.
5. From the zero-shear viscosity (η_o) vs volume fraction of solids (ϕ) plot the aspect ratio p = (diameter/thickness) $\cong$ 287 $\pm$ 9 of the dispersed clay particles was calculated, in agreement with value computed from relative permeability, p = 286.
6. Calculated number of end-tethered, spaced about 1.2 nm apart, PA-6 macromolecules to a single clay platelet is ca. 140,000. Owing to the trans-reaction between these hairy clay platelets and PA-6 the molecular weight of the end-tethered macromolecules increases. This is consistent with the different effect PNC has on dG′/dt and dG″/dt (see 1, above). It also provides explanation as to why addition of $\phi = 0.0064$ of clay to PA-6 resulted in doubling η_o and increasing of ψ_o by a factor of 160.

Acknowledgements The authors express thanks to Mr. P. Sammut for the rheological tests and discussions of the results.

References

Bureau M (2001) Mechanical behavior and crack propagation in injection molded polyamide-6/clay nanocomposites. SPE Technical Paper 47 (in press)

Clarey M, Edwards J, Tsipursky SJ, Beall GW, Eisenhour DD (2000) Method of manufacturing polymer-grade clay for use in nanocomposites. US Pat 6,050,509 to Amcol International

Dagani R (1999) Putting the "nano" into composites. Chem Eng News 77(23):25–37

Deguchi R, Nishio T, Okada A (1992) Polyamide composite material and method for preparing the same. US Pat 5,102,948 to Ube Industries Ltd and Toyota Jidosha Kabushiki Kaisha, Aichi, Japan

Doi M, Edwards SF (1978) J Chem Soc Faraday Trans 2(74):1802–1818

Galgali G, Ramesh C, Lele A (2001) A rheological study on the kinetics of hybrid formation in polypropylene nanocomposites. Macromolecules 34:852–858

Gilman JW, Kashiwagi T, Morgan AB, Harris RH Jr, Brassel L, van Landingham M, Jackson CL (2000) Flammability of polymer clay nanocomposites consortium: year one report. U.S. Department of Commerce, NISTR No 6531

Hoffmann B, Dietrich C, Thomann R, Friedrich C, Zilg C, Mülhaupt R (2000a) Macromol Rapid Commun 21:57–61

Hoffmann B, Kressler J, Stöppelmann G, Friedrich C, Kim G-M (2000b) Rheology of nanocomposites based on layered silicates and polyamide-12. Colloid Polym Sci 278:629 – 636

Khanna YP, Han PK, Day ED (1996) New developments in the melt rheology of nylons. I. Effect of moisture and molecular weight. Polym Eng Sci 36:1745–1754

Knudson MI Jr, Jones TR (1992) Process for manufacturing organoclays having enhanced gelling properties. US Pat 5,110,501 to Southern Clay Products

Krishnamoorti R, Giannelis EP (1997) Rheology of end-tethered polymer layered silicate nanocomposites. Macromolecules 30:4097–4102

Krishnamoorti R, Vaia RA, Giannelis EP (1996) Structure and dynamics of polymer-layered silicate nanocomposites. Chem Mater 8:1728–1734

Okada A, Usuki A (1995) The chemistry of polymer-clay hybrids. Mater Sci Eng C3:109–115

Okada A, Fukushima Y, Kawasumi M, Inagaki S, Usuki A, Sugiyama S, Kurauchi T, Kamigaito O (1988) Composite material and process for manufacturing same. US Pat 4,739,007 to Kabushiki Kaisha Toyota Chou Kenkyusho, Aichi, Japan

Okamoto M, Nam PH, Maiti P, Kotaka T, Hasegawa N, Usuki A (2001) A house of cards structure in polypropylene/clay nanocomposites under elongational flow. Nano Lett 1:295–298

Piggott MR (1980) Load bearing fibre composites. Pergamon, Oxford

Ren J, Silva AS, Krishnamoorti R (2000) Linear viscoelasticity of disordered polystyrene-polyisoprene block copolymer based layered-silicate nanocomposites. Macromolecules 33:3739–3746

Schmidt G, Nakatani AI, Butler PD, Karim A, Han CC (2000) Shear orientation of viscoelastic polymer-clay solutions probed by flow birefringence and SANS. Macromolecules 33:7219–7222

Simha R (1940) The influence of Brownian movement on the viscosity of solutions. J Phys Chem 44:25–34

Solomon MJ, Almusallam AS, Seefeldt KF, Somwangthanaroj A, Varadan P (2001) Rheology of polypropylene/clay hybrid materials. Macromolecules 34:1864–1872

Takahashi T (1996) PhD Thesis, Yamagata University, Yonezawa, Japan

Ube Industries (2000) High performance nylon resin – technical data. Ube Industries, Nylon Resin Dept

Utracki LA (1984) Polymer blends and alloys for molding applications. Polym-Plast Technol Eng 22:27–54

Utracki LA (1989) Polymer alloys and blends. Hanser, Munich

Utracki LA (1995) The rheology of multiphase systems. In: Covas JA, Agassant JF, Diogo AC, Vlachopoulos J, Walters K (eds) Rheological fundamentals of polymer processing. Kluwer Academic Publishers, Dordrecht, pp 113–137

Utracki LA, Kamal MR (2002) Clay-containing polymeric nanocomposites. Arabian J Sci Eng (accepted)